

*The effect of noise on pitchfork and Hopf  
bifurcations*

Juel, A. and Darbyshire, A.G. and Mullin, T.

1997

MIMS EPrint: **2007.129**

Manchester Institute for Mathematical Sciences  
School of Mathematics

The University of Manchester

Reports available from: <http://eprints.maths.manchester.ac.uk/>

And by contacting: The MIMS Secretary  
School of Mathematics  
The University of Manchester  
Manchester, M13 9PL, UK

ISSN 1749-9097

# The effect of noise on pitchfork and Hopf bifurcations

BY ANNE JUEL<sup>1</sup>†, ALAN G. DARBYSHIRE<sup>1</sup> AND TOM MULLIN<sup>2</sup>

<sup>1</sup>*Department of Atmospheric, Oceanic and Planetary Physics,  
Clarendon Laboratory, University of Oxford, Parks Road, Oxford OX1 3PU, UK*

<sup>2</sup>*Schuster Laboratory, University of Manchester, Manchester M13 9PL, UK*

We present the results of an experimental and numerical investigation of the effects of noise on pitchfork and Hopf bifurcations. Good quantitative agreement is found between calculations and experiment. In the case of the pitchfork we find that natural imperfections override the effects of the noise. However, novel noise amplification effects have been uncovered in the study of the Hopf bifurcation. These destroy the critical event found in the noise-free case and could be of considerable practical importance in systems containing dynamic bifurcations.

---

## 1. Introduction

The dynamical state of a physical system can be considered to consist of a deterministic part together with the effects of internal or external random fluctuations. In most cases, this leads to small variations about a deterministic state but near critical events such as bifurcations, the system can show great sensitivity to small scale random perturbations. The effect of noise on critical phenomena has been of great interest in statistical physics and nonlinear optics for a number of years (see, for instance, Graham 1973). More recently, the concepts have been applied to chaotic systems as reviewed in the monograph by Horsthemke & Lefever (1984). They focus on non-intuitive events such as noise-induced transitions, where interactions between deterministic dynamics and random perturbations result in a broad range of novel dynamical phenomena.

The present combined experimental and numerical study is concerned with the effects of small additive random perturbations in the form of white noise on codimension-one bifurcations from a fixed point. Specifically, we have studied the effects of additive noise on the dynamics near supercritical Hopf and pitchfork bifurcations. In these transitions the singly peaked probability distribution of the noise is split into a bimodal one as a bifurcation point is passed. The experimental system we use consists of a high-quality nonlinear electronic oscillator which has a very low inherent noise level. In a previous theoretical and numerical study, Healey *et al.* (1991) show that a codimension-two organizing centre for the dynamics is formed by a Hopf and pitchfork bifurcation. Specifically, they find that period-doubling routes

† Present address: Schuster Laboratory, University of Manchester, Manchester M13 9PL, UK.

to chaos form parts of Silnikov homoclinic orbits. The relevant details of the circuit are described in §2 where we also discuss the numerical methods.

The stability of pitchfork symmetry-breaking bifurcations subject to random external fluctuations is of relevance to a number of practical applications and numerous studies have been reported. Among these, Ariaratnam & Xie (1992) find that noise has a destabilizing effect so that the critical value of the parameter is reduced compared to the noise free case. In practice, however, the bifurcation is disconnected by the presence of small naturally occurring imperfections. An experimental study by Kondepuki *et al.* (1986) and a combined theoretical and numerical one by Kondepuki (1989) show that when the imperfection parameter is weaker than the magnitude of the noise, the disconnection has a profound influence on the dynamics depending on the rate that the control parameter is swept through the bifurcation. In particular, the probability of reaching the connected state increases with the magnitude of the disconnection parameter and decreases when the sweeping rate is raised. Watson & Reiss (1982) report on the effects of noise on the connected branch of an imperfect pitchfork bifurcation using a statistical approach and find a scatter around the averaged solution curve. The amount of broadening is greatest in the vicinity of the critical value of the parameter corresponding to the perfect bifurcation. The broadening appears because time scales of perturbations become very long at a bifurcation point. This phenomenon is often referred to as critical slowing down by analogy with critical phenomena in phase transitions as discussed by Pfister & Gerds (1981).

In the present work, we have adopted an alternative approach to the effects of noise on bifurcations which focuses on the dynamical behaviour of the system. Specifically, we investigate the dynamics of the system using modern ideas from nonlinear time series analysis and in doing so have uncovered some novel noise induced dynamics. We begin our study with the pitchfork bifurcation in both its connected and disconnected form and a combination of numerical and experimental results is reported in §3. We then compare and contrast the results obtained for the pitchfork bifurcation with those observed with a Hopf bifurcation.

Interesting novel dynamical behaviour which was found as a precursor to the Hopf bifurcation from a steady state in the presence of noise is discussed in §4*a*. Similar effects are reported by Schöpf & Rehberg (1992) who studied convective instabilities in binary-fluid mixtures although they attribute them to spatial wave instabilities. Evidence of fluctuations is also discussed by Fronzoni *et al.* (1987) in their study of an analogue electronic circuit model of the Brusselator. Wiesenfeld (1985) reports different classes of ‘noisy precursors’ which are also a direct consequence of nearby bifurcations of periodic orbits subject to external perturbations. Theoretical predictions by Wiesenfeld & McNamara (1986) concerning the amplification of periodic perturbations near a critical event are confirmed experimentally by Martin & Martienssen (1987). They investigated small signal amplification in the vicinity of a Hopf bifurcation found in the electrical conductivity of barium sodium niobate single crystals. They show that for small amplitude excitations, the system follows linear theory but for large amplitudes, the response is nonlinear and the spread of the fluctuations is independent of the bifurcation parameter.

In both the Hopf and the symmetry-breaking bifurcations, a shift in the critical value of the parameter is potentially of significant practical importance and hence, it has been investigated by several authors. Namachchivaya & Ariaratnam (1987) find that the Hopf bifurcation point can be shifted in either direction using a Markov diffusion process. Altares & Nicolis (1988) show that the Hopf bifurcation is systematically postponed under stochastic forcing using a Fokker–Planck approach. Similarly,

Hoffman (1982) reports that the onset of the limit cycle is spread over a parameter interval rather than arising at a precise critical value. The width and position of the interval depends on the noise power. In a similar vein, Zhu & Yu (1987) point out that noise has the effect of smearing out two-peak distributions found near the bifurcation point. Finally, Kabashima & Kawabuko (1979) report an experimental observation of a noise-induced phase transition in a parametric oscillator, where the external noise both shifts the bifurcation point and modifies the properties of the oscillation near its threshold. In §4*b*, we investigate the shift in the Hopf bifurcation point using a statistical approach and a method involving the fast Fourier transform and show empirically that the magnitude of the shift as well as its direction depend on the method employed. Results from the numerical simulations are presented in parallel with the experimental study and show that the noise tends to smear out the bifurcation as seen from the study of the dynamics in the vicinity of the bifurcation point. We comment on our results and compare and contrast the qualitative differences between the Hopf and pitchfork bifurcations in §5.

## 2. Experimental methods and numerical procedure

The experiments were performed using a modified Van der Pol LCR oscillator which contains variable nonlinear elements in the feedback circuit. A schematic circuit diagram is presented in figure 1. The behaviour of the system was controlled by the settings on the two variable resistances which determine the magnitude of the nonlinearities. These are in turn used to define the axes on a control parameter plane. Details of the circuit together with the results of an extensive theoretical and experimental study of the dynamical behaviour can be found in Healey *et al.* (1991). They show that homoclinic orbits, of Silnikov type, underpin the period-doubling sequences to chaos. The fundamental components which combine to give the observed Silnikov dynamics are pitchfork and Hopf bifurcations. These two codimension-one bifurcations were the subject of the present study where noise was injected into the circuit as shown in figure 1. The particular point of injection was selected since it was found that the external noise circuit had minimal effect on other characteristics of the oscillator, so that the impedance matching of the noise circuit and the nonlinear oscillator resulted in small parameter changes of less than 0.5%.

Initial results suggested that long-term small amplitude drift in the output voltage was significant near bifurcation points. It had a timescale of hours and was mainly caused by heating of the diodes which formed the positive nonlinear conductance since all other components had high-temperature stability. The problem was overcome by attaching a thermal bath to the base of the oscillator and thermally insulating the remainder of the system. The temperature of the bath was kept constant to within 0.02 °C using a commercial circulator so that the long-term drift was effectively eliminated.

The noise generator comprises of a high-quality electronic random-number generator which produces a random sequence of zeros and ones where each digit is generated at a fixed clock rate. Thus the lowest frequency is determined by the length of the sample and the upper limit is set by the clock rate so that the bandwidth is 1 MHz with a flat spectrum over the range. However, when the noise generator was connected to the oscillator, the characteristics of the noise were modified in two ways. Firstly, the high  $Q$  of the resonant circuit severely colours the noise with a roll off around 150 Hz which is the centre frequency of the oscillator. As we shall see later,

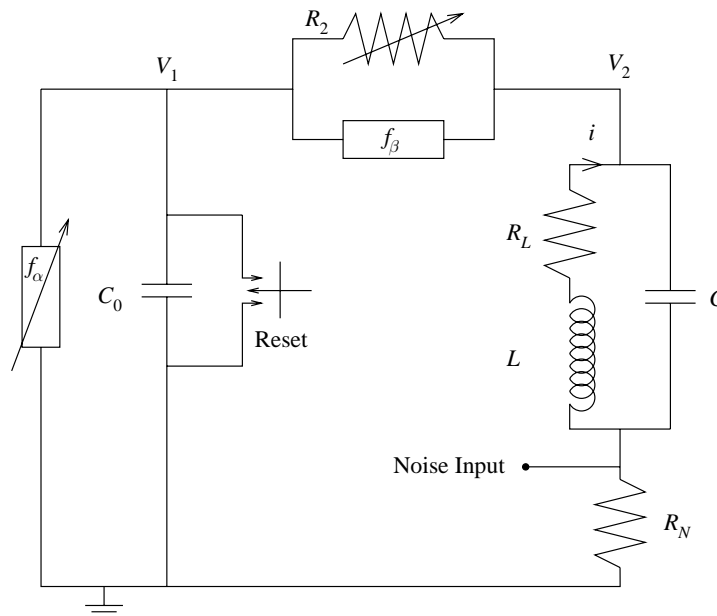


Figure 1. Schematic diagram of the electronic circuit.

this was not as big a problem as one might intuitively expect since the dominant features near bifurcation points are controlled by time scales which are much longer than this. This observation was supported by the numerical results where the effective bandwidth is an order of magnitude greater than in the experiment. Secondly, when the noise source is connected to the oscillator, the RMS amplitude of the noise signal is reduced compared to that measured when the generator is disconnected. This effect was taken into account when comparing with the numerical results.

When the system was disconnected from the noise source a very small amount of 50 Hz interference from the mains supply to the laboratory was observed. This contamination was reduced using a battery supply and suitable orientation of the inductor coil. However, it could not be completely eradicated although its contribution was of an order of magnitude less than the added noise. There is no such contribution in the numerical model and good agreement between the experiment and numerical simulations discussed in §§3 and 4 shows that the mains' effect is not significant.

Also, our experimental system is not, of course, strictly 'noise free'. The inherent noise level in the oscillator was determined by retaining the background level of the power spectrum at a fixed point. It was found to be approximately 2.5 orders of magnitude smaller than that measured when the noise generator was connected to the oscillator.

The system is governed by the following non-dimensional equations which have been derived using Kirchoff's laws:

$$\dot{x} = \gamma[f_\beta(y - x) - f_\alpha(x)], \quad (2.1 a)$$

$$\dot{y} = -z - f_\beta(y - x), \quad (2.1 b)$$

$$\dot{z} = y - \rho z, \quad (2.1 c)$$

where the nonlinear conductances are modelled to cubic order using the relations

$$f_\alpha(v) = -\alpha_1 v + \alpha_3 v^3, \quad (2.2 a)$$

$$f_\beta(v) = \beta_1 v + \beta_3 v^3. \quad (2.2 b)$$

The position of the Hopf bifurcation in the system of equations was calculated using the numerical bifurcation solver AUTO developed by Doedel (1986). The parameter values ( $\alpha_1$ ,  $\beta_1$  and  $\beta_3$ ) can be calculated directly from the experimental settings. The value of the parameter  $\alpha_3$  in the circuit was estimated using the position of the quartic point where the nature of the Hopf bifurcation changes from supercritical to subcritical as discussed by Healey *et al.* (1991). The actual value of  $\alpha_3$  does not affect the position of the Hopf bifurcation; however, too low a value changes the qualitative form of the bifurcation from supercritical to subcritical and hence made the integration of the solution beyond the bifurcation point difficult.

A stochastic term,  $\epsilon(t)$ , was introduced into equation (2.1 *c*) in an additive manner which simulates the way the noise is injected in the experiment. Equation (2.1 *c*) then becomes

$$\dot{z} = y - \rho z + \epsilon(t). \quad (2.3)$$

It is, of course, not known if this models all the details of the experimental situation but the close correlation between experimental and numerical results suggests that this is an appropriate way to simulate the injection of the noise into the circuit. We also subjected the equations to multiplicative noise where it was appropriate and did not uncover any significant difference.

The numerical noise was generated from a Gaussian probability distribution with zero mean and RMS amplitude,  $\sigma$ . The equations were integrated using an implicit method where the value of the noise term,  $\epsilon(t)$ , was held constant during the integration time step,  $\Delta t$ . This procedure limits the effective bandwidth of the noise but it is an order of magnitude greater than that used in the experiment as discussed above. In all the integrations  $\Delta t$  was set to  $10^{-1}$  in non-dimensional units, which is equivalent to a sampling rate of 11.6 kHz.

In order to make direct comparisons between the experiment and the numerical integrations, the amplitude of the noise term in the equation was set to be of the same order as that used in the experiment. The amplitude of the noise added in the experiment was estimated by measuring the RMS amplitude of the signal at a point in parameter space well below the Hopf bifurcation point. Then the amplitude of a limit cycle was measured in the experiment with no added noise at a point in parameter space some way above the bifurcation point. The equations were also integrated with  $\sigma = 0$ , and hence  $\epsilon(t) = 0$ , at the same point in parameter space. The ratio of the measured and the calculated magnitudes of the limit cycles gives a scaling factor between the measured noise level and the amplitude of the noise to be added to the equations. This led to a value,  $\sigma = 10^{-2}$ , being chosen as the additive noise level in the numerical integrations.

### 3. The pitchfork bifurcation

In this section, we examine the effect of noise on both a perfect and an imperfect symmetry-breaking bifurcation. The latter is encountered in practice where imperfections present in all physical systems cause the disconnection of the bifurcation (Golubitsky & Schaeffer 1985). The imperfections in the electronic oscillator originate from different sources and their effect was modelled in the numerical simulations

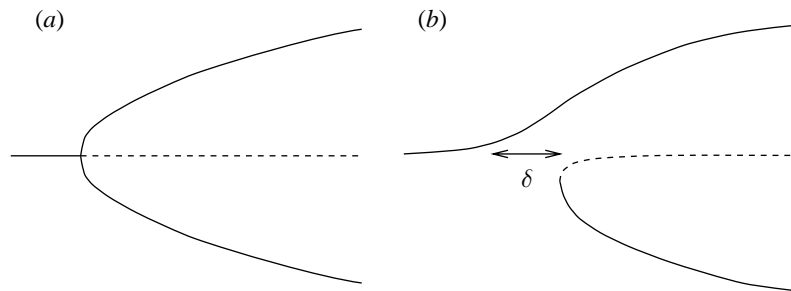


Figure 2. Schematic representation of a perfect (a) and imperfect (b) pitchfork bifurcation.

by adding a static disconnection term,  $\delta$ , to equation (2.1 *b*). Schematic diagrams of the perfect and imperfect pitchfork bifurcations are presented in figure 2.

As will be shown below, the study of the perfect case allowed us to compare and contrast the results with those obtained for the Hopf bifurcation while the imperfect case enabled us to make a direct comparison with results from the oscillator. In the following,  $\alpha_1$  is chosen as the bifurcation parameter and its critical value is denoted by  $\alpha_{1cp}$  for the perfect pitchfork while  $\alpha'_{1cp}$  gives the position of the saddle-node point resulting from the disconnection of the bifurcation.

In all cases, the initial condition of the integration was set to be the origin. In order to visualize the effect of noise on the symmetry-breaking bifurcation, normalized probability distributions of the amplitude of the solution were estimated using the computed time series. For a perfect noise-free system, the probability distributions evolve from a single Dirac delta function at zero amplitude for  $\alpha_1 < \alpha_{1cp}$  to two such functions at a pair of symmetric finite values of the amplitude for  $\alpha_1 > \alpha_{1cp}$ . However, in the added-noise case the distributions will have finite width which will be greatest at the bifurcation point. All of the discussion below will be concerned with the case of added noise unless otherwise stated.

#### (a) *The perfect pitchfork bifurcation*

A series of probability distributions are shown in figure 3. Each one was calculated for both the perfect and the imperfect pitchfork bifurcation from numerically integrated time series, comprising  $1.5 \times 10^7$  samples in total. We present the distributions of the perfect and the imperfect cases together to aid the discussion.

We will first discuss the results of the numerical study of the case of a perfect pitchfork bifurcation. The corresponding distributions are drawn in figure 3 with rhombi. The distribution shown in figure 3*a* was formed from a time series calculated at  $\alpha_1/\alpha_{1cp} = 9.973 \times 10^{-1}$ . Here the probability distribution of the noise is broadened by a factor of four due to the reduction of the damping in the vicinity of the bifurcation point. The distribution shown in figure 3*b* was formed at  $\alpha_1/\alpha_{1cp} = 1$ . It can be seen that the width of the probability distribution is now greater than that shown in figure 3*a* and it is also flattened on top. This is because large time scales dominate the dynamics at the bifurcation point. Indeed, an infinitely long time series would be required to obtain a true estimate of the distribution, since the transient behaviour of the system scales with  $1/(\alpha_{1cp} - \alpha_1)$ . The distributions corresponding to the successively supercritical values of  $\alpha_1/\alpha_{1cp}$  equal to, respectively, 1.002, 1.005 and 1.007 are shown in figures 3*c–e*. It can be seen that the system alternates between the two stable symmetric solution branches. The distributions hence consist of two peaks centred at symmetric positions connected together by a channel. The width

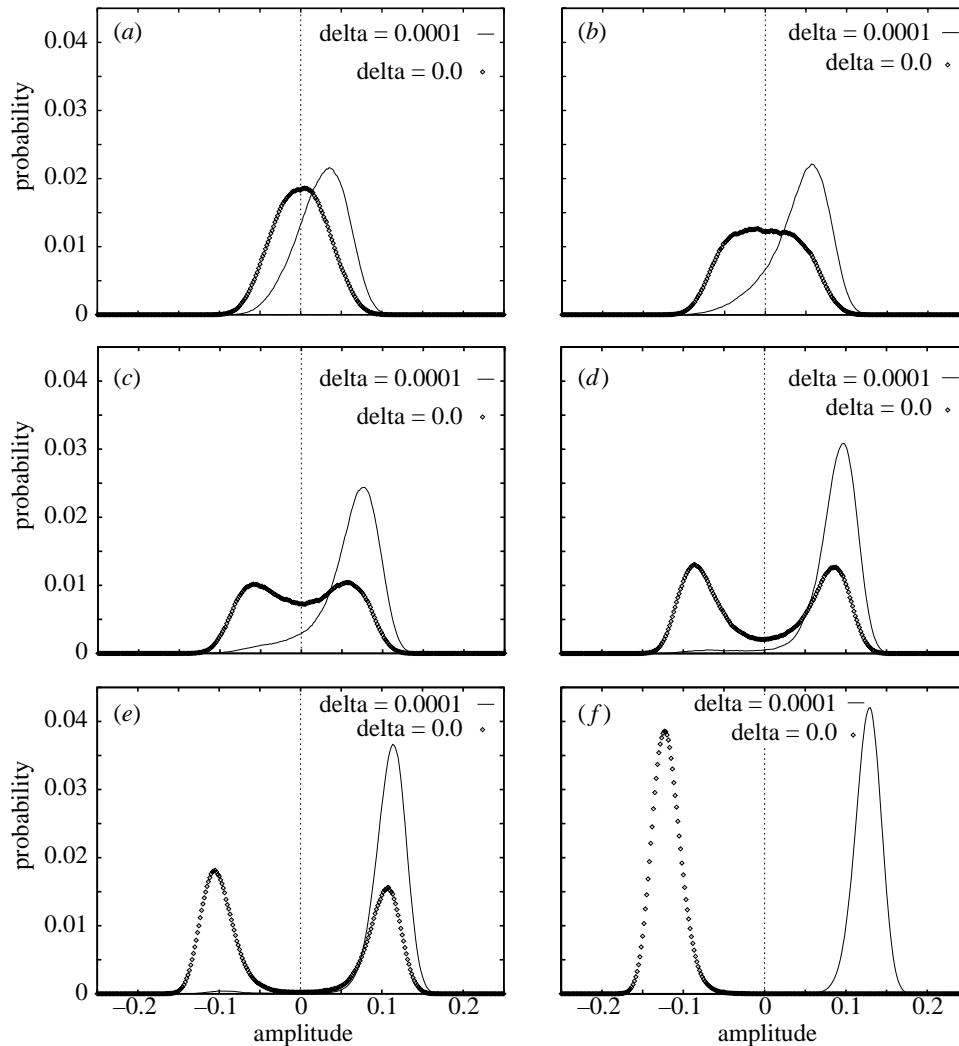


Figure 3. Numerical probability distributions represented by rhombi for the perfect pitchfork bifurcation and solid lines for the imperfect one: (a)  $\alpha_1/\alpha_{1cp} = 9.973 \times 10^{-1}$ ; (b)  $\alpha_1/\alpha_{1cp} = 1$ ; (c)  $\alpha_1/\alpha_{1cp} = 1.002$ ; (d)  $\alpha_1/\alpha_{1cp} = 1.005$ ; (e)  $\alpha_1/\alpha_{1cp} = 1.007$ ; and (f)  $\alpha_1/\alpha_{1cp} = 1.010$ .

of the channel between the two peaks narrows as  $\alpha_1$  increases so that transition between the two solution branches becomes less and less likely as the parameter is increased. Hence long time scales again become important in the formation of the distribution. This phenomenon is often referred to as the first passage time problem and more details can be found in the textbook by Van Kampen (1992).

The apparent asymmetry in the amplitude of the peaks observed as  $\alpha_1$  is increased is a direct result of the passage time effect, i.e. the integrations would have to be run for longer and longer times to achieve equality of the peak amplitudes. However, the ratio of peaks was always found to tend to one for long enough time steps in the vicinity of the bifurcation point. When  $\alpha_1$  is further increased as in figure 3f where  $\alpha_1/\alpha_{1cp} = 1.010$  the peaks become more distinct and in practice, the system settles onto a particular stable branch although in principle there is a finite probability that it can reach the other state. Thus, the probability distribution is again Gaussian but

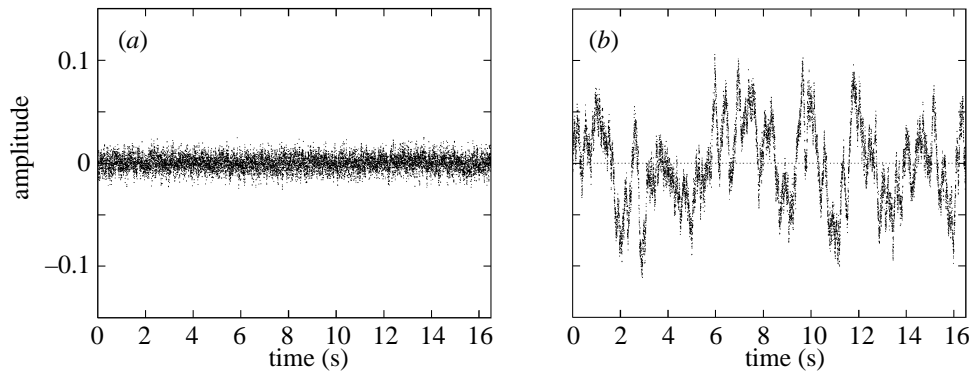


Figure 4. Numerical time series in the case of a perfect pitchfork bifurcation with added noise: (a)  $\alpha_1/\alpha_{1cp} = 0.5$ ; (b)  $\alpha_1/\alpha_{1cp} = 1$ .

now centred on one or other of the branches. Hence, the symmetry of the bifurcation is not broken by the addition of noise to the system. However, the noise interacts with long-time-scale dynamics at the bifurcation point and introduces large time scale variations in the resulting time series. This can be seen in figure 4 where two time series calculated for  $\alpha_1/\alpha_{1cp} = 0.5$  (figure 4a) and  $\alpha_1/\alpha_{1cp} = 1$  (figure 4b) are compared.

The critical value of the parameter can be evaluated from the probability distributions by determining the distance between either peak and the origin as a function of supercritical values of  $\alpha_1$ . This distance corresponds to the distance between either branch of the pitchfork and the trivial solution and, thus, varies as the square root of the excess parameter so that the critical value of the parameter can in principle be estimated. The method was applied to the distributions shown in figures 3c–f and the critical value of the parameter was found to remain located at  $\alpha_{1cp}$ .

#### (b) *The imperfect pitchfork bifurcation*

The electronic oscillator is a very well controlled experiment but, as in the case of any physical system, the presence of imperfections is inevitable. In the present case, the effect of the imperfections is much smaller than is typically found in other physical systems as discussed by Mullin & Cliffe (1986). Hence, if the critical dynamics found in the abstract perfect case are to be of relevance to the physical situation then detectable phenomena ought to be found in the numerical model when a small imperfection term is added. In order to check this, we carried out tests with a range of imperfections in the model and found no evidence for critical dynamics. We have decided to present results with the disconnection parameter,  $\delta$ , set to  $10^{-4}$  to emphasize this point since this value is approximately one order of magnitude smaller than in the experiment.

The probability distributions for the imperfect case are plotted as thin solid lines in figure 3. In the subcritical case shown in figure 3a, the distribution can be seen to be asymmetric even with the small imperfection term. The probability distribution is slightly broadened at the base when  $\alpha_1/\alpha_{1cp} = 1$ , due to the underlying dynamics which result from the remnants of the pitchfork bifurcation. All supercritical distributions have a bias so that the distribution is centred on the connected branch. As  $\alpha_1$  is increased a second branch appears which is disconnected. It can be seen in figure 3e that even with this small imperfection, the probability of reaching the disconnected state is exceptionally small so that we have not observed this sponta-

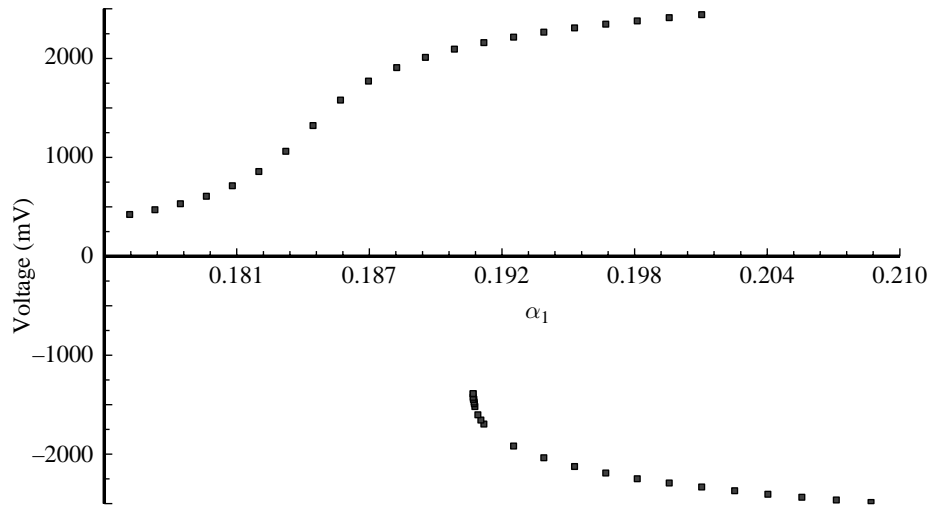


Figure 5. Experimental pitchfork bifurcation diagram with added noise. It is indistinguishable from that measured in the 'noise-free' case.

neous transition in the numerical simulations. However, when the system was given an appropriate initial condition so that it reached the disconnected branch, it was found to remain in this state.

In the imperfect case there is no critical event, as a parameter is smoothly swept up and down so that the system follows the connected solution. However, a practical measure of a pitchfork can be made by observing the critical value of the saddle-node bifurcation. This can be done in practice by jumping to the disconnected state and then reducing the control parameter. If the disconnection is small, as it is here, then a good estimate of the pitchfork bifurcation of the perfect model can be obtained.

The experimental disconnected pitchfork bifurcation diagram was reconstructed with and without noise added to the system. The noise level was the same as that applied in the numerical simulations. Each experimental point was determined by retaining the mean value of times series comprising  $10^5$  points and sampled at a rate of 1000 Hz. The bifurcation diagrams were undistinguishable when superimposed and data sampled with the noise generator connected is displayed in figure 5. However, a careful study of the disconnected branch close to the saddle-node bifurcation point showed that the critical value of  $\alpha_1$  was systematically reduced by less than 0.1% compared to the 'noise-free' case. This shift is small and is indistinguishable from the slight parameter change, caused by the impedance matching of the noise circuit and the nonlinear oscillator.

Probability distributions were constructed from the experimental time series used in the bifurcation diagram of figure 5. Noise added to the system smooths out the probability distribution at the fixed point so that it becomes a broadened Gaussian distribution as discussed in §2. Probability distributions taken from the disconnected branch close to the saddle-node point are shown superimposed in figure 6. In the 'noise-free' system, the saddle-node point is located at  $\alpha'_{1cp}$ . For  $\alpha_1/\alpha'_{1cp} = 1.0025$ , 1.0011 and 1.0003, only a very small broadening of the distributions is observed. However, for  $\alpha_1/\alpha'_{1cp} = 1.0000$ , distinct broadening is found due to the long-time-scale dynamics of the critical point as discussed above.

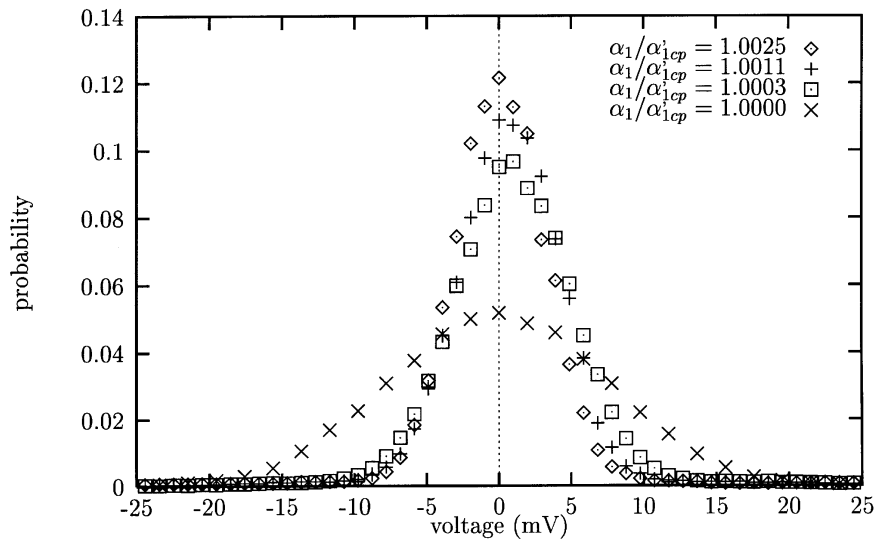


Figure 6. Experimental probability distributions from the disconnected branch close to the saddle-node point. In each case the mean has been removed so that all distributions are centred on zero.

#### 4. The Hopf bifurcation

Experimental results of the effect of noise on a Hopf bifurcation are potentially much more interesting since this is a dynamic critical event which cannot be unfolded by the presence of physical imperfections. Indeed, initial observations of time series sampled in the vicinity of the bifurcation point showed particularly interesting novel features such as significant noise amplification which is discussed in §4*a*. Another feature, which has been extensively reported in the literature, is that the presence of noise can produce a shift in the critical value of the bifurcation parameter (Namachchivaya & Ariaratnam 1987; Altares & Nicolis 1988; Hoffman 1982; Zhu & Yhu 1987; Kabashima & Kawakubo 1979). However, we show in §4*b* that the measure used to determine bifurcation points can lead to apparently conflicting results in both the experimental and numerical investigations.

##### (*a*) Dynamics close to the bifurcation point

In this section we discuss experimental and numerical observations of the dynamics found in the vicinity of a Hopf bifurcation in the presence of noise. In all of the present results the parameter  $\beta_1$  in equation (2.2*b*) is fixed,  $\alpha_1$  is used as the bifurcation parameter and its critical value is denoted by  $\alpha_{1cH}$ . Experimental time series were sampled at a rate of 300 Hz for different values of  $\alpha_1$  either side of the bifurcation point of the ‘noise-free’ system. The sampling rate corresponds to twice the frequency of the oscillation which arises at the Hopf bifurcation, is approximately 150 Hz and while it does not provide a good measurement of the oscillation, the long-time-scale dynamics close to the bifurcation region are clearly represented. Experimental time series were sampled over a period of 180 s and examples are shown in figures 7*a–f*. They correspond to the parameter values  $\alpha_1/\alpha_{1cH} = 6.373 \times 10^{-1}$ ,  $9.522 \times 10^{-1}$ ,  $9.746 \times 10^{-1}$ ,  $9.862 \times 10^{-1}$ ,  $9.981 \times 10^{-1}$  and 1.001, respectively and were recorded after switching  $\alpha_1$  instantaneously from a small value where the solution was a steady state to the given values.

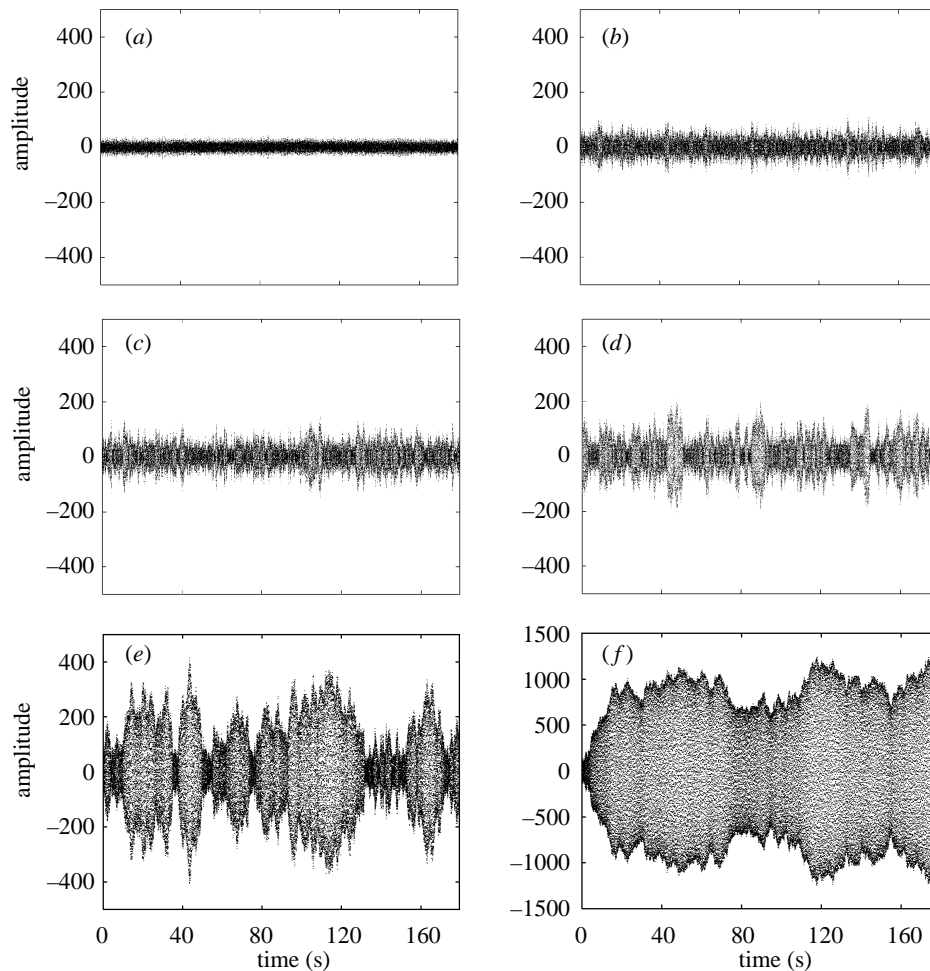


Figure 7. Experimental time series in the vicinity of a Hopf bifurcation: (a)  $\alpha_1/\alpha_{1cH} = 6.373 \times 10^{-1}$ ; (b)  $\alpha_1/\alpha_{1cH} = 9.522 \times 10^{-1}$ ; (c)  $\alpha_1/\alpha_{1cH} = 9.746 \times 10^{-1}$ ; (d)  $\alpha_1/\alpha_{1cH} = 9.862 \times 10^{-1}$ ; (e)  $\alpha_1/\alpha_{1cH} = 9.981 \times 10^{-1}$ ; and (f)  $\alpha_1/\alpha_{1cH} = 1.001$ .

The experimental time series displayed in figure 7a was taken far below the bifurcation point and the small level of added noise is present. A detailed study of the time series showed that it was strongly coloured around 150 Hz. As  $\alpha_1$  is progressively increased (figures 7a–e), low-frequency variations appear in the form of correlated oscillations in the envelope of the time series. Both the characteristic time scale and amplitude of these variations increase as  $\alpha_1$  is increased towards the critical value. In the time series displayed in figures 7b–e, the system oscillates about the zero volts state. However, the one shown in figure 7f, where  $\alpha_1$  is set 0.06% above its critical value in the unperturbed case and which was sampled using the same procedure as for the previous ones, appears to be a transient growth from the trivial solution to the oscillatory one since the low-frequency amplification of the noise persists but at a non-zero amplitude. However, there is in principle a finite probability that the noise can perturb the system back onto the trivial branch and, thus, this time series should still be considered to display low-frequency variations on a characteristic time scale which is much longer than the sampled data record. Alternatively, the amplification

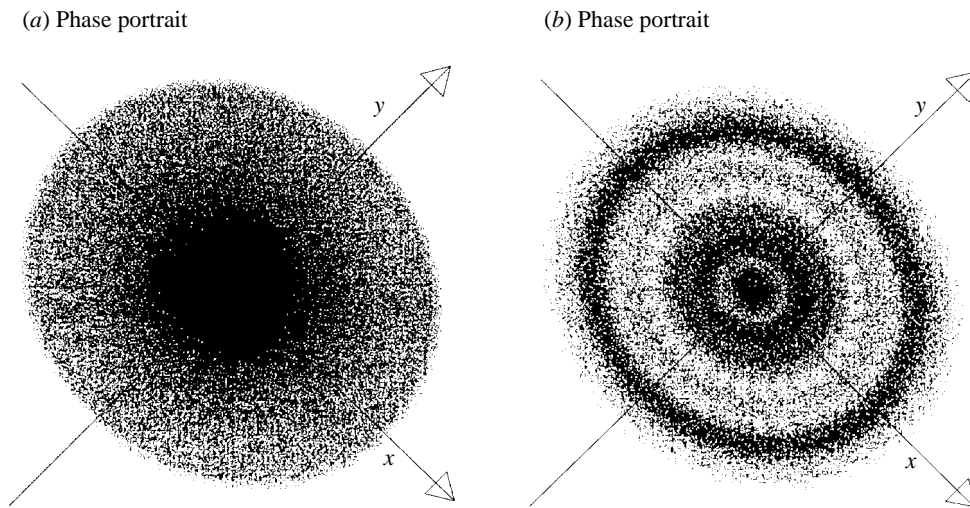


Figure 8. Experimental phase portraits of transient time series just beyond  $\alpha_{1cH}$  in the 'noise-free' case (a) and just below  $\alpha_{1cH}$  in the case of added noise (b).

of the noise as the bifurcation point is approached could be described as arising from a reduction of the damping. The noise level in the system is constant and the damping associated with the stable fixed point restricts the noisy trajectory to a small neighbourhood of the trivial solution. As the bifurcation point is approached the damping decreases, the trajectory becomes less constrained and hence explores a larger neighbourhood of the fixed point leading to an apparent amplification of the noise.

Further analysis was carried out on the experimental data by reconstructing phase portraits using the singular value decomposition technique proposed by Broomhead & King (1986). We show two examples of these in figure 8 from transient time series which were sampled by switching the parameter from a subcritical to a small supercritical value, respectively, without and with noise. When the external noise source is disconnected, the solution stays close to the fixed point for a very long time since here the system is only just supercritical and thus the time constant is large. It then spirals out uniformly towards the final limit cycle corresponding to the periodic orbit. The phase portrait only shows the initial transient so that the limit cycle is outside of the displayed record. In the case of added external noise, the solution is almost immediately kicked off the fixed point. It then spirals locally in and out, tends to stabilize temporarily at certain amplitudes before it is kicked off and starts spiralling out again. It finally reaches a limit cycle, represented by the outer dark circle in figure 8b, which is broadened due to the effect of the noise.

Numerical results were calculated for values of  $\alpha_1$  so that the ratios  $\alpha_1/\alpha_{1cH}$  corresponded to those used in the experiment and shown in figure 7. In each case the initial condition of the integration was taken to be the origin of statespace. A sequence is shown in figure 9 of six time series of the  $x$  variable as  $\alpha_1$  is increased towards the critical value. Each series contains  $5 \times 10^5$  points so that, in real time, they correspond to a quarter of the length of the experimental set shown in figure 7. It can be seen that there is a striking similarity between the experimental and the numerical results. As the bifurcation point is approached from below, the interaction between the applied noise and the dynamics of the bifurcating limit cycle results in

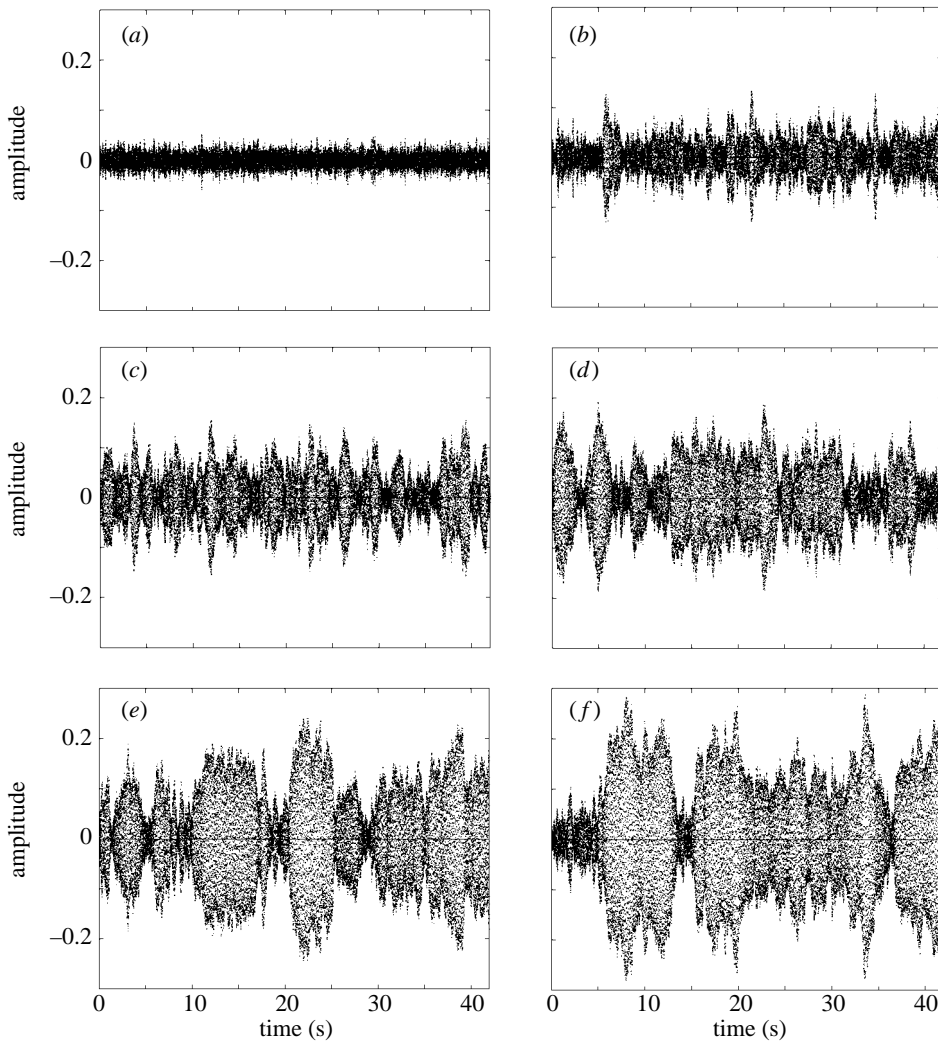


Figure 9. Numerical time series in the vicinity of a Hopf bifurcation: (a)  $\alpha_1/\alpha_{1cH} = 6.375 \times 10^{-1}$ ; (b)  $\alpha_1/\alpha_{1cH} = 9.508 \times 10^{-1}$ ; (c)  $\alpha_1/\alpha_{1cH} = 9.742 \times 10^{-1}$ ; (d)  $\alpha_1/\alpha_{1cH} = 9.862 \times 10^{-1}$ ; (e)  $\alpha_1/\alpha_{1cH} = 9.962 \times 10^{-1}$ ; and (f)  $\alpha_1/\alpha_{1cH} = 1.0014$ .

the introduction of increasingly long time scales into the time series. However, there are interesting differences between the experimental time series shown in figure 7 and those of figure 9. The sequence in figure 9 shows a steady increase in amplitude while a qualitative change occurs between figures 7*e*, *f*. The time series displayed in figures 7*f* and 9*f* were sampled very close to the critical point where the characteristic time scales are very large and the precise state of the system appears to depend on details in the noise. Thus, this remains an unresolved issue and further work is needed to understand the behaviour of the system at the bifurcation point.

The above integrations were carried out in order to simulate the procedure used in the experiment. An alternative method was also applied where the periodic orbit produced by the Hopf bifurcation was used as the initial condition and then noise was added. A typical time series, calculated at  $\alpha_1/\alpha_{1cH} = 1.0014$ , is shown in figure 10 and is to be compared with figure 9*f*. Both time series are very similar at this small

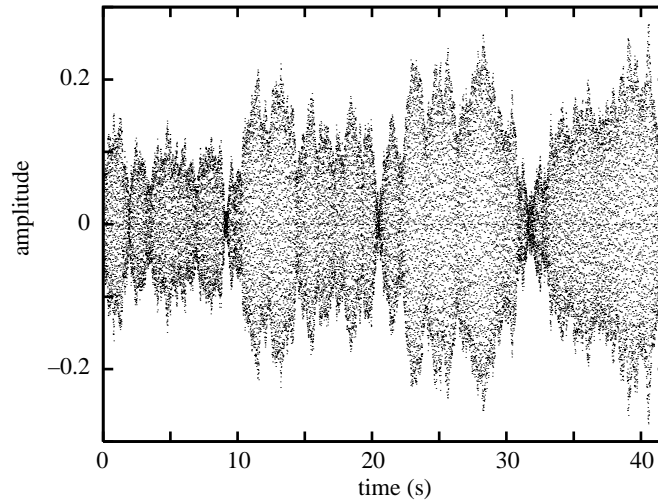


Figure 10. Numerical time series at  $\alpha_1/\alpha_{1cH} = 1.0014$  where the initial condition is the Hopf limit cycle.

value of the excess parameter. This suggests that the observed behaviour is not a transient which will eventually dissipate.

We next investigated the possibility that this long-time-scale dynamical behaviour was a special property of this particular oscillator. In order to do this we repeated the above integration procedure with a pair of ordinary differential equations which can be shown to undergo a Hopf bifurcation at  $\rho = 0$  as discussed by Drazin (1992).

$$\dot{u} = -v + u(\rho - u^2 - v^2), \quad (4.1a)$$

$$\dot{v} = u + v(\rho - u^2 - v^2). \quad (4.1b)$$

Again a Gaussian noise term is added to one of the equations so that equation (4.1b) becomes

$$\dot{v} = u + v(\rho - u^2 - v^2) + \epsilon(t). \quad (4.2)$$

The parameter  $\sigma$  was set to  $5 \times 10^{-3}$  and the integration was performed the same way as described above, with an integration time step  $\Delta t = 10^{-1}$  and the initial condition set to be the origin. A sequence of time series of the  $u$  variable comprising of  $5 \times 10^5$  points and calculated for values of  $\rho$  between  $-5 \times 10^{-2}$  and  $1 \times 10^{-3}$  is shown in figure 11. Here the bifurcation occurs at  $\rho = 0$ . Again the scenario observed in the experiment and the integration of the oscillator equations is found. Thus, as the bifurcation point is approached, time scales much longer than the period of the periodic orbit or of that of the added noise are contained in the dynamics of the system.

Finally, Healey *et al.* (1991) showed that there exist Hopf bifurcations in this oscillator on the non-trivial symmetry broken states. A similar investigation to the above of these Hopf bifurcations again shows time series remarkably similar to the sequence described in the experiment. In addition, these bifurcations were also investigated using multiplicative noise and the same qualitative features were found.

(b) *Shift in the critical value of the bifurcation parameter*

Both the perfect and imperfect cases of the pitchfork bifurcation have been considered and no significant change has been found in the critical values of the parameter.

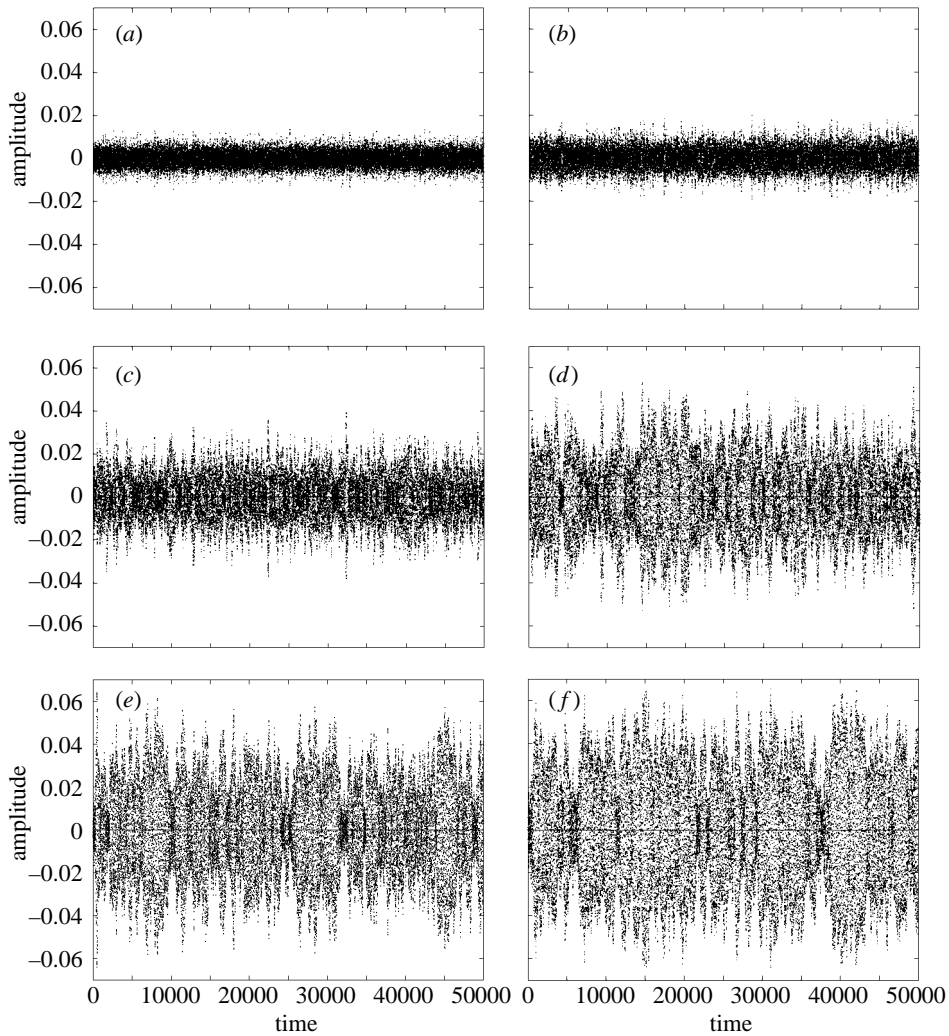


Figure 11. Time series from the integration of the normal form of a Hopf bifurcation: (a)  $\rho = -5.0 \times 10^{-2}$ ; (b)  $\rho = -2.5 \times 10^{-2}$ ; (c)  $\rho = -5.0 \times 10^{-3}$ ; (d)  $\rho = -1.0 \times 10^{-3}$ ; (e)  $\rho = 0.0$ ; and (f)  $\rho = 1.0 \times 10^{-3}$ .

In the case of a perfect pitchfork bifurcation, we used probability distributions to characterize the transition and showed that, far enough beyond the critical event, they followed a square-root dependence in agreement with the noise-free bifurcation. In the imperfect case, we showed experimentally in figure 5 that the bifurcation diagram remained unchanged when noise was added to the system. We now use these techniques to characterize the more interesting effects of noise on the dynamics of the Hopf bifurcation.

Experimentally, the investigation was carried out by studying the transient behaviour of the system as it evolves from a fixed point to a limit cycle. The growth of the transients can be modelled by the Landau equation of the form

$$A(t) = \sqrt{\frac{A_e^2 e^{2t/\tau}}{e^{2t/\tau} + (A_e/A_i)^2 - 1}}, \quad (4.3)$$

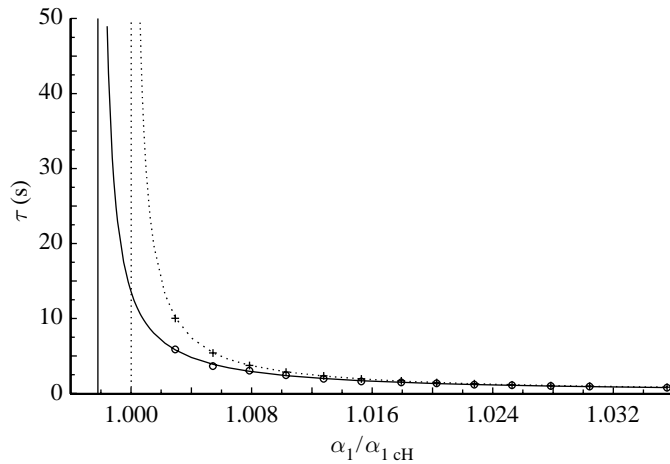


Figure 12. Hyperbolic fit to experimental Landau time constants determined at small values of the excess parameter in the ‘noise-free’ case (dashed line) and when noise is added to the system (solid line). The critical value of the parameter is determined in each case from the vertical asymptotes.

where  $\tau$  is the growth time of the transient,  $A_i$  the initial amplitude and  $A_e$  the final amplitude of the signal. This approach was used by Pfister & Gerdtz (1981) to show critical slowing down close to a Hopf bifurcation in the flow between concentric cylinders commonly called the Taylor–Couette problem. The growth time is itself a function of the parameter value  $\alpha_1$  of the form

$$\tau = \frac{\tau_0}{\alpha_1 - \alpha_{1cH}} = f(\alpha_1), \quad (4.4)$$

where  $\alpha_{1cH}$  is the critical value of  $\alpha_1$  and  $\tau_0$  a constant. The growth time,  $\tau$ , was determined for several values of  $\alpha_1$  in order to reconstruct the function  $\tau = f(\alpha_1)$  and thus extrapolate the critical value  $\alpha_{1cH}$ . In principle, a more robust estimation of  $\alpha_{1cH}$  could be obtained by measuring a series of decay rates for  $\alpha_1 < \alpha_{1cH}$  in addition to the growth rates. However, the design of the oscillator did not allow a systematic study of the decaying transients and thus, the investigation was restricted to growing ones alone.

It was more difficult to determine growth times close to the bifurcation point in the case of added noise since the envelopes of the time series contained long time scale variations as discussed in §4*a*. A systematic reduction of the critical value of the parameter was found for three different levels of noise applied as shown by the results presented in figure 12 for the level of noise adopted in the simulations. Crosses represent the data from the ‘noise-free’ system while the corresponding hyperbolic fit is drawn as a dashed line. In the case of added noise, the data points are represented by empty circles while the hyperbolic fit is drawn as a solid line. The vertical lines (dashed for the ‘noise-free’ case and solid in the case of added noise) show the positions of the extrapolated bifurcation points. The shift was found to be of 0.2% towards subcriticality which is at the limit of experimental and fitting uncertainties.

Another method commonly used to determine the critical value of the parameter for a Hopf bifurcation involves the fast Fourier transform. The height of the dominant peak in the power spectrum is measured and related to the amplitude of the oscillation. The plot of power versus the parameter  $\alpha_1$  should be linear since the amplitude varies as the square root of the excess parameter. Thus the critical value

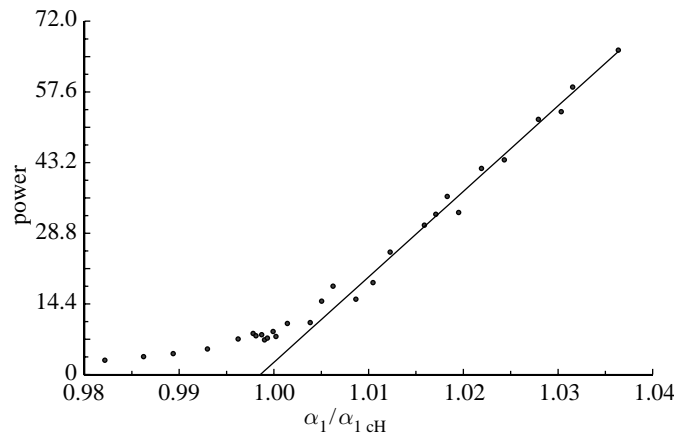


Figure 13. Power in the vicinity of a Hopf bifurcation calculated from numerical time series with added noise. A least-squares fit to the points of significant power suggests that the critical value of the parameter is shifted by 0.32% towards subcriticality.

of  $\alpha_1$  can be extrapolated using a linear regression. This method was first applied to numerical data calculated in the presence of noise. It can be seen from figure 13 that the bifurcation point is smeared out since the plot of power against the parameter  $\alpha_1$  does not follow a linear law close to the bifurcation point. A least-squares fit to the data where there is significant power suggests that the bifurcation point is virtually shifted towards subcriticality by 0.32%.

This method was also used on a set of experimental measurements and the results are shown in figure 14. They were taken in the vicinity of the Hopf bifurcation on the connected asymmetric branch at  $\beta_1 = 1.879 \times 10^{-1}$  alternatively with and without noise. The time series comprised  $4 \times 10^5$  points which were sampled at a rate of 1000 Hz. The data points without noise are represented by solid circles to which a solid straight line is fitted. The data points taken in the case of injected noise are shown by empty circles with a dashed straight line fitted to them. In the absence of added noise, all the data points beyond the critical value of  $\alpha_1$  approximately form a straight line except for the ones immediately past  $\alpha_{1cH}$  since no physical system is strictly noise free. Thus, in the experimental situation, the effects observed numerically in figure 13 are expected to be less pronounced so that the bifurcation point needs to be approached more closely. This last point ties in with the differences observed between the experimental and numerical time series in the vicinity of the Hopf bifurcation, shown in figures 7 and 9, which were discussed in § 4 *a*. When noise is added to the system, the data in the immediate vicinity of the bifurcation point, both in subcritical and supercritical regions, show a smooth increase which becomes linear only at a certain distance from  $\alpha_{1cH}$ . This effect is due to the long-time-scale dynamics which amplifies the noise in the immediate vicinity of the bifurcation point and effectively smears it out; i.e. each of the low-frequency envelopes comprises a randomly modulated oscillation at the frequency which will be present above the Hopf bifurcation point. Hence the peak in the power spectrum grows smoothly as the parameter is increased.

As stated above, this effect applies to a considerably smaller interval of values of  $\alpha_1$  than that encountered in the numerical simulations. The estimate of  $\alpha_{1cH}$  is shifted towards supercriticality by 0.06%. However, the injection of the noise in the experimental system results in a slight change in the parameters as discussed in § 3 *b*.

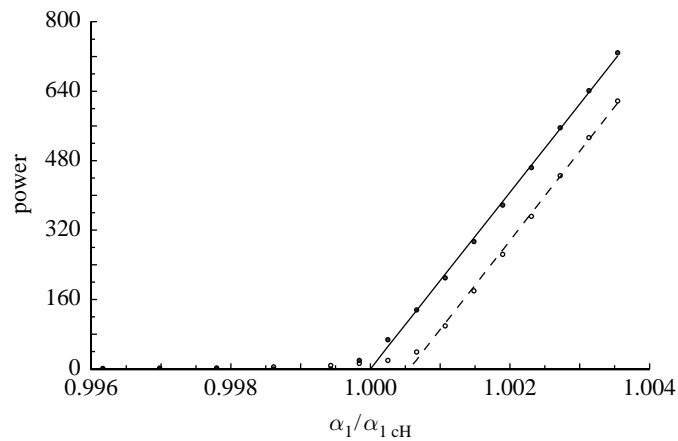


Figure 14. Power in the vicinity of a Hopf bifurcation calculated from experimental time series with (empty circles and dashed line) and without added noise (solid circles and solid line). The least square fit to the noisy data is shifted with respect to the 'noise-free' one. This is due to a slight change in the parameter values caused by the connection of the noise source.

This parameter change can be taken into account by translating the dashed line which fits the measurements taken in the presence of noise onto the solid one so as to make the experimental results directly comparable with the numerical ones. The two straight lines are parallel and, thus, superimpose so that no significant change in the value of the critical parameter  $\alpha_{1cH}$  is observed.

The bifurcation point can also be estimated by calculating amplitude probability distributions from sets of time series as in the case of the pitchfork bifurcation. For the Hopf bifurcation, the probability distribution consists of a single peak centred on zero amplitude in the subcritical state where the system is at a fixed point. It then splits into two symmetrically dispersed peaks after the bifurcation. The distance between peaks can then be determined as a function of  $\alpha_1$  as the bifurcation point is approached. The inter-peak distance corresponds to the amplitude of the limit cycle and thus varies as the square root of the parameter  $\alpha_1$ . The position of the bifurcation point can then in principle be estimated. However, when noise is added to the system, the bifurcation point is smeared out which results in a broadening and flattening of the amplitude distribution very close to the bifurcation point. It is therefore difficult to determine accurately when the transition to the oscillatory state occurs and in many common experimental situations the accuracy would be very difficult to achieve. In figure 15, the bifurcation curve calculated in the noise-free case is plotted as a solid line together with numerical inter-peak distances as functions of  $\alpha_1/\alpha_{1cH}$ . A square-root fit, drawn as a dashed line in figure 15, was used to estimate the bifurcation point which was found to be shifted by 0.43% towards supercriticality.

Experimentally, probability distributions were determined from the time series previously used for the calculations of figure 14. In figure 16, a series of probability distributions for  $\alpha_1/\alpha_{1cH} = 9.9984 \times 10^{-1}$ , 1.0002, 1.0007, 1.0011 and 1.0019 illustrate the transition from a single- to a double-peaked distribution. It should be noted that the experiment shows an apparent delay in the critical event as in the case of the numerical results. These results are in agreement with those of Kabashima & Kawabuko (1979).

It could be argued that since we are concerned with noise-related phenomena

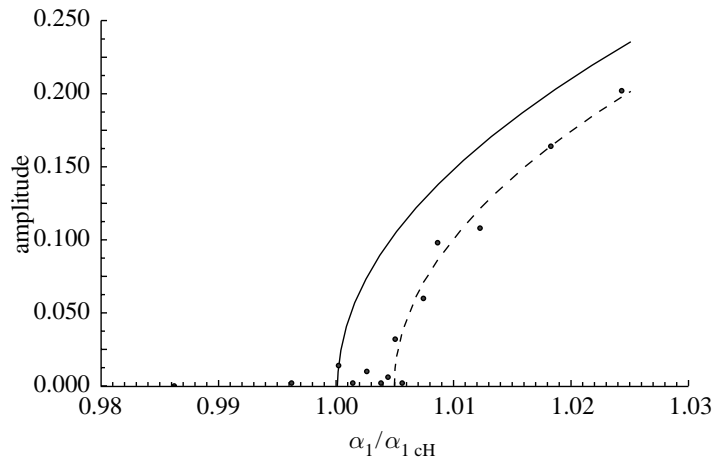


Figure 15. Numerical Hopf bifurcation curve and inter-peak distances in the case of added noise. The estimated value of the critical value of the parameter is shifted by 0.43% towards supercriticality.

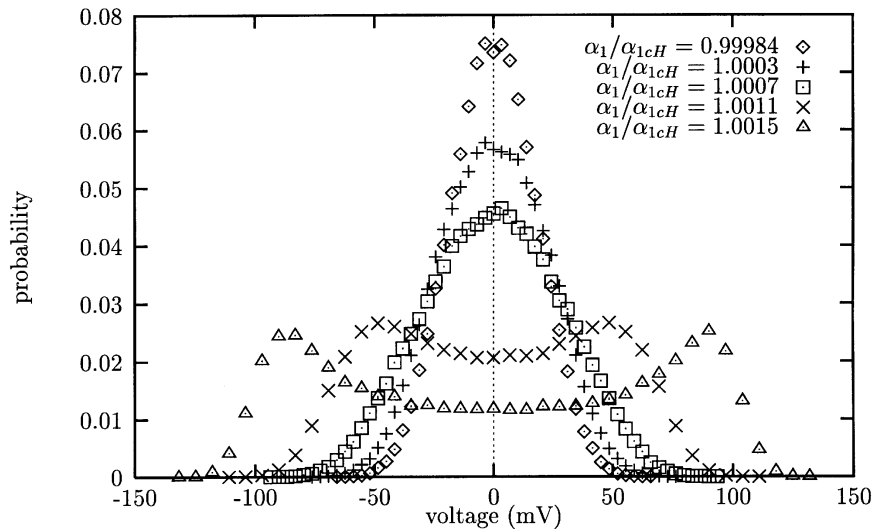


Figure 16. Experimental probability distributions in the vicinity of a Hopf bifurcation.

then the statistical approach of constructing probability distributions provides the best approach. However, the transition from a single to a double peak is a smooth process and the long-term dynamics near the origin dominates close to the critical point. Hence it is difficult in practice to ascribe a critical parameter value at which the distribution splits. In addition, the peaks in the double distribution are not Gaussian and hence the simple measure of the distance between their maxima is not an accurate indicator of the amplitude of the oscillation: similarly, the amplitude of the peak in the power spectral density representation is affected by the noise. Hence we conclude that there is no significant shift in the Hopf bifurcation point but that there are very interesting long-term dynamics induced which smears out the critical event of the 'noise-free' system.

## 5. Conclusion

We have presented a combined experimental and numerical investigation of the effect of added noise on codimension-one bifurcations from a fixed-point solution.

Comparison was made numerically between the perfect and imperfect pitchfork bifurcation which showed no significant shift in the critical value of the parameter in either case. However, long-time-scale dynamics were found at the bifurcation point in the perfect case. Experimentally, a slight broadening of the probability distributions was obtained at the saddle-node point and no significant long-term dynamics were observed.

Long-time-scale-correlated oscillations were found as precursors to Hopf bifurcations both experimentally and numerically. These are qualitatively distinct from those found in the case of the pitchfork since oscillations at the Hopf frequency are always present and the long-time-scale dynamics takes the form of random modulations. This effect does not appear to have been discussed in the literature and could be of considerable practical importance since it involves significant amplification of small-scale noise at subcritical parameter values. The integration of the normal form of a Hopf bifurcation showed that this effect may be present in a wide range of systems. In the presence of noise, the critical value of the parameter was determined using three different methods. Small deviations from  $\alpha_{1cH}$  in either direction were obtained, due to the long-time-scale dynamics mentioned above. Thus, ‘new’ dynamics are introduced in the system by the presence of noise which causes the Hopf bifurcation to become dynamically imperfect.

The authors thank Dr Robin Jones for the use of the electronic noise generator and the oscillator: we are grateful to both him and Professor Dave S. Broomhead for many useful discussions. The support of the Defence Research Agency at Malvern (A.J.) is gratefully acknowledged. We also thank one of the referees for reading the original manuscript with particular care and making many helpful suggestions.

## References

- Altares, V. & Nicolis, G. 1988 Stochastically forced Hopf bifurcation: approximate Fokker-Planck equation in the limit of short correlation times. *Phys. Rev. A* **37**, 3630–3633.
- Ariaratnam, S. T. & Xie, W. 1992 Sensitivity of pitchfork bifurcation to stochastic perturbations. *Dyn. Stability Syst.* **7**, 139–150.
- Broomhead, D. S. & King, G. P. 1986 Extracting qualitative dynamics from experimental data. *Physica D* **20**, 217–236.
- Doedel, E. 1986 AUTO: software for continuation and bifurcation problems in ordinary differential equations. Applied mathematics reports, California Institute of Technology.
- Drazin, P. 1992 *Nonlinear systems*. Cambridge University Press.
- Fronzoni, L., Mannella, R., McClintock, P. V. E. & Moss, F. 1987 Postponement of Hopf bifurcations by multiplicative colored noise. *Phys. Rev. A* **36**, 834–841.
- Golubitsky, M. & Schaeffer, D. G. 1985 *Singularities and groups in bifurcation theory*. New York: Springer.
- Graham, R. 1973 *Statistical theories of instabilities in stationary nonequilibrium systems with applications to lasers and nonlinear optics*. Springer Tracts in Modern Physics, no. 66. Berlin: Springer.
- Healey, J. J., Broomhead, D. S., Cliffe, K. A., Jones, R. & Mullin, T. 1991 The origins of chaos in a modified Van der Pol oscillator. *Physica D* **48**, 322–339.
- Hoffman, K. H. 1982 The Hopf bifurcation of two-dimensional systems under the influence of one external noise source. *Z. Phys. B* **49**, 245–252.

- Horsthemke, W. & Lefever, R. 1984 *Noise-induced transitions*. Berlin: Springer.
- Kabashima, S. & Kawakubo, T. 1979 Observation of a noise-induced phase transition in a parametric oscillator. *Phys. Lett. A* **70**, 375–376.
- Kondepuki, D. K. 1989 State selection dynamics in symmetry-breaking transitions. *Noise in nonlinear dynamical systems*. (ed. F. Moss & P. V. E. McClintock). Cambridge University Press.
- Kondepuki, D. K., Moss, F. & McClintock, P. V. E. 1986 Observation of symmetry-breaking, state selection and sensitivity in a noisy electronic system. *Physica D* **21**, 296–306.
- Martin, S. & Martienssen, W. 1987 Resonance behaviour near Hopf bifurcations in the electrical conductivity of BSN crystals. *Z. Phys. B* **68**, 299–304.
- Mullin, T. & Cliffe, K. A. 1986 Symmetry-breaking and the onset of time-dependence in fluid mechanical systems. *Nonlinear phenomena and chaos* (ed. S. Sarkar). Bristol: Hilger.
- Namachchivaya, N. S. & Ariaratnam, S. T. 1987 Stochastically perturbed Hopf bifurcation. *Int. J. Nonlinear Mech.* **22**, 363–372.
- Pfister, G. & Gerdts, U. 1981 Dynamics of Taylor wavy vortex flow. *Phys. Lett. A* **83**, 19–22.
- Schöpf, W. & Rehberg, I. 1992 Amplification of thermal noise via convective instability in binary-fluid mixtures. *Europhys. Lett.* **17**, 321–326.
- Van Kampen, N. G. 1992 *Stochastic processes in physics and chemistry*. North-Holland: Elsevier.
- Watson, J. G. & Reiss, E. L. 1982 A statistical theory for imperfect bifurcation. *SIAM J. Appl. Math.* **42**, 135–148.
- Wiesenfeld, K. 1985 Noisy precursors of nonlinear instabilities. *J. Stat. Phys.* **58**, 1071–1097.
- Wiesenfeld, K. & McNamara B. 1986 Small signal amplification in bifurcating dynamical systems. *Phys. Rev. A* **33**, 629–642.
- Zhu, W.-Q. & Yhu, J. S. 1987 On the response of the van der Pol oscillator to white noise excitation. *J. Sound Vibration* **117**, 421–431.

*Received 22 October 1996; revised 13 March 1997; accepted 21 May 1997*

